

# Polarization Behavior and Corrosion Inhibition of Copper in Acidic Chloride Solution Containing Benzotriazole

Sang Hee Suh<sup>†</sup> and Youngjoon Suh

*Suh and Suh Corrosion Engineering, Dongpangyo 156, 907-901, Bundang-gu, Seongnam Gyunggi-do 13524, Republic of Korea*  
(Received February 17, 2023; Revised May 02, 2023; Accepted May 03, 2023)

Polarization behavior and corrosion inhibition of copper in acidic chloride solutions containing benzotriazole were studied. Pourbaix diagrams constructed for copper in NaCl solutions with different BTAH concentrations were used to understand the polarization behavior. Open circuit potential (OCP) depended not only on chloride concentration, but also on whether a CuBTA layer was formed on the copper surface. Only when the (pH, OCP) was located well in the CuBTA region of the Pourbaix diagram, a stable corrosion inhibiting CuBTA layer was formed, which was confirmed by X-ray Photoelectron Spectroscopy (XPS) and a long-term corrosion test. The OCP for the CuBTA layer decreased logarithmically with increasing [Cl<sup>-</sup>] activity in the solution. A minimum BTAH concentration required to form a CuBTA layer for a given NaCl concentration and pH were determined from the Pourbaix diagram. It was found that 320 ppm BTAH solution could be used to form a corrosion-inhibiting CuBTA layer inside the corrosion pit in the sprinkler copper tube, successfully reducing water leakage rate of copper tubes. These experimental results could be used to estimate water chemistry inside a corrosion pit.

**Keywords:** Benzotriazole, Copper, Chloride, Polarization, Pourbaix diagram

## 1. Introduction

Copper has been used widely for many applications requiring corrosion resistance, thanks to the naturally formed thin oxide layer on the copper surface playing as a passivating layer. However, in acidic chloride solutions, copper loses its corrosion resistance due to dissolution of the passivating oxide layer [1,2]. Copper is also prone to pitting corrosion in high pH water in presence of chlorine [3–6]. The small space of the corrosion pit under the corrosion products is filled with an acidic solution possibly containing chloride, accelerating corrosion of the corrosion pit [7]. Taxén [8,9] could obtain the profiles of pH, potential, and concentration of various chemical species inside the copper corrosion pit by a model study. The low pH values of around 3 and the high activity of Cu<sub>2</sub>O and CuCl were predicted near the bottom of the corrosion pit. The authors of the current study [10] also found by XPS and EDS analyses of corrosion pits that the bottom of the corrosion pit consists of Cu<sub>2</sub>O and CuCl layers, indicative of high concentrations of chloride and cuprous species present in

the solution inside the corrosion pit. Lee et al. [11] also found by Energy Dispersive Spectroscopy (EDS) and X-ray Photoelectron Spectroscopy (XPS) analyses that localized corrosion and Cl concentration occurred at the carbonaceous film–copper boundary due to crevice corrosion.

BTAH (Benzotriazole, C<sub>6</sub>H<sub>5</sub>N<sub>3</sub>) has been used for more than 70 years as one of the most effective corrosion inhibitors for copper and its alloys [12]. When copper is immersed in a BTAH solution, a passivating layer of polymerized CuBTA complex is formed rapidly on the copper surface [13,14]. The CuBTA layer is known to be effective in inhibiting corrosion of copper in acidic and chloride solutions [15,16]. Kosec et al. reported that BTAH plays as an excellent corrosion inhibitor of not only copper but also for brass in chloride solution [17]. However, there are reports that BTAH becomes ineffective in the NaCl solution at pH lower than 3 [18,19]. There have been few reports on whether BTAH could be effective for either stopping or delaying propagation of corrosion pits already formed on copper. Lee et al. [11] found that when BTAH was added to the test solution, a CuBTA complex was formed at the boundary of the carbonaceous film to prevent localized corrosion. The current authors studied

<sup>†</sup>Corresponding author: [suhanduh@outlook.kr](mailto:suhanduh@outlook.kr)  
Sang Hee Suh: CEO, Youngjoon Suh: Technical Manager

using oxygen scavengers such as hydrazine [20] and sodium sulfite [21] to reduce water leakage caused by the pitting corrosion of the sprinkler copper tubing. They could not observe noticeable decrease in water leakage by using oxygen scavengers. On the other hand, using BTAH [10,22], they could reduce the water leakage from sprinkler copper tubes by more than 80% and they found a strong dependency of the water leakage frequency on the BTAH concentration.

The motivation of this study is to find the reason why the corrosion inhibition of copper by BTAH strongly depends on its concentration in a highly acidic and chloride containing aqueous solution like the one in the corrosion pit. The authors examined the polarization behavior and corrosion inhibition of copper electrodes immersed in acidic NaCl solutions at various pH values with different BTAH concentrations. Formation of the corrosion inhibiting CuBTA layer on copper was studied by EDS and XPS. They tried to understand the polarization behavior and corrosion inhibition by referring to the Pourbaix diagrams (potential vs. pH diagram) constructed for these solutions.

## 2. Experimental procedures

A master BTAH aqueous solution of 10,000 ppm was used to make test solutions of 100, 300, 600 ppm BTAH. The purity of BTAH (CAS No. 95-14-7) used was better than 99%, as specified by the manufacturer, Samchun Chemicals of Korea. The chloride concentration and pH value of the solutions was adjusted by adding NaCl and citric acid to the solutions. The NaCl concentrations investigated are from 0.01 M to 1 M. The pH value was varied between 2.5 and 7.4.

The potentiodynamic polarization tests were carried out to obtain the polarization curves of copper working electrodes in the test solutions. A copper sticky tape 10 mm wide and 0.1 mm thick with adhesive on the back was used as the copper working electrode. The copper tape was firmly bonded to a 0.2 mm thick PVC sheet and the opening of  $1 \times 1 \text{ cm}^2$  was made by masking it with a scotch tape. The purity of the copper tape was better than 99.95% by weight. The naturally formed copper oxide on the copper tape was not removed before the test. The copper electrode was tested after immersed in the test solution for 5 hours. A saturated calomel electrode and a

graphite rod of 5 mm in diameter were used as the reference electrode and the counter electrode, respectively. WonATech's WPG100 Potentiostat and Smart Interface were used for the measurements with a scanning rate of 5 mV/s. The potentials were reported in the results with respect to the saturated calomel electrode potential ( $V_{\text{SCE}}$ ) which is 0.242 V smaller than the standard hydrogen electrode ( $V_{\text{SHE}}$ ). A long term corrosion test was also performed by immersing copper tape specimens for 2.3 years in the 1 M NaCl solutions at pH around 3.9 with different BTAH concentrations from 0 to 600 ppm.

EDS and XPS analyses of the specimens were carried out by Korea Institute of Science and Technology's Advanced Analysis and Data Center. A Hitachi Regulus 8230 was used for the EDS analysis with the acceleration voltage of 5 kV. An Ulvac-PHI's PHI 5000 VersaProbe was used for the XPS analysis. The X-ray source for XPS was monochromatic Al K $\alpha$  with the beam spot size of  $100 \mu\text{m} \times 100 \mu\text{m}$ .

## 3. Results and Discussion

### 3.1 Pourbaix diagram of Cu-Cl-BTAH-H<sub>2</sub>O system

Tromans [23] constructed for the first time the Pourbaix diagrams of copper in acidic and acidic/chloride aqueous solutions containing BTAH. Tromans and Sun used these diagrams to interpret the anodic polarization curves of copper in BTAH-added acidic NaCl solutions [18]. In the current study, Pourbaix diagrams at 25 °C of the Cu-Cl-BTAH-H<sub>2</sub>O system of 1 M and 0.1 M NaCl aqueous solutions (Fig. 1 and Fig. 2) were constructed in the pH interval between 1 and 8 in which BTAH is the predominant phase over either BTA<sup>-</sup> or BTAH<sub>2</sub><sup>+</sup>. The equilibrium potentials and equilibrium constants summarized in Table 1 were used for these constructions. These thermodynamic equilibrium equations and data were obtained from the data by Tromans [23] and Bertocci and Wagman [24]. Activity coefficients of 0.66 and 0.78 were used to calculate the activities of chloride in the 1 M and 0.1 M NaCl solutions, respectively [25]. The BTAH concentrations of 100, 300, and 600 ppm were used for the Pourbaix diagram in the 1 M NaCl solution, while only the 300 ppm BTAH concentration was used for the Pourbaix diagram in the 0.1 M NaCl solution. The boundary line position between the CuBTA and Cu

**Table 1. Thermodynamic data for Cu-Cl-BTAH-H<sub>2</sub>O system at 25 °C [23,24]**

Equilibrium equations	Equilibrium potentials, E (V <sub>SHE</sub> ) or equilibrium constants, K for the left equilibrium equations		
$\text{CuBTA} + \text{H}^+ + \text{e}^- = \text{Cu} + \text{BTAH}$	(1a)	$E = 0.0946 - 0.0591 \log [\text{BTAH}] - 0.0591 (\text{pH})$	(1b)
$\text{Cu}^{2+} + \text{BTAH} + \text{e}^- = \text{CuBTA} + \text{H}^+$	(2a)	$E = 0.5861 + 0.0591 (\text{pH}) + 0.0591 \log [\text{Cu}^{2+}] + 0.0591 \log [\text{BTAH}]$	(2b)
$\text{CuO} + \text{BTAH} + \text{H}^+ + \text{e}^- = \text{CuBTA} + \text{H}_2\text{O}$	(3a)	$E = 0.975 - 0.0591 (\text{pH}) + 0.0591 \log [\text{BTAH}]$	(3b)
$\text{CuCl}_2 \cdot 3\text{Cu}(\text{OH})_2 + 4\text{BTAH} + 2\text{H}^+ + 4\text{e}^- = 4\text{CuBTA} + 6\text{H}_2\text{O} + 2\text{Cl}^-$	(4a)	$E = 0.805 - 0.02955 \log [\text{Cl}^-] + 0.0591 \log [\text{BTAH}] - 0.02955\text{pH}$	(4b)
$4\text{Cu}^{2+} + 6\text{OH}^- + 2\text{Cl}^- = \text{CuCl}_2 \cdot 3\text{Cu}(\text{OH})_2$	(5a)	$K = 2.0 \times 10^{69}$	(5b)
$4\text{CuO} + 2\text{H}^+ + 2\text{Cl}^- + \text{H}_2\text{O} = \text{CuCl}_2 \cdot 3\text{Cu}(\text{OH})_2$	(6a)	$K = 3.7 \times 10^{11}$	(6b)
$\text{CuBTA} + \text{Cl}^- + \text{H}^+ = \text{CuCl} + \text{BTAH}$	(7a)	$K = 0.4243$	(7b)
$\text{CuCl} + \text{e}^- = \text{Cu} + \text{Cl}^-$	(8a)	$E = 0.116 - 0.0591 \log [\text{Cl}^-]$	(8b)
$\text{Cu}^{2+} + \text{Cl}^- + \text{e}^- = \text{CuCl}$	(9a)	$E = 0.567 + 0.0591 \log [\text{Cu}^{2+}] + 0.0591 \log [\text{Cl}^-]$	(9b)
$\text{Cu}^{2+} + \text{H}_2\text{O} = \text{CuO} + 2\text{H}^+$	(10a)	$K = 2.69 \times 10^{-7}$	(10b)
$\text{Cu}^{2+} + 2\text{Cl}^- + 2\text{e}^- = \text{CuCl}_2$	(11a)	$E = 0.457 + 0.118 \log [\text{Cl}^-]$	(11b)

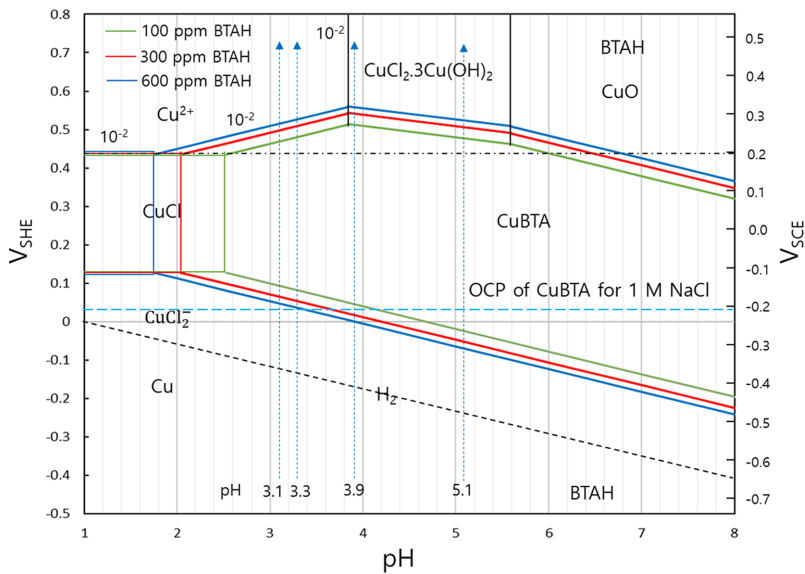


**Fig. 1. Pourbaix diagram for Cu-Cl-BTAH-H<sub>2</sub>O system in the presence of 1 M NaCl and 10<sup>-2</sup> M Cu<sup>2+</sup>**

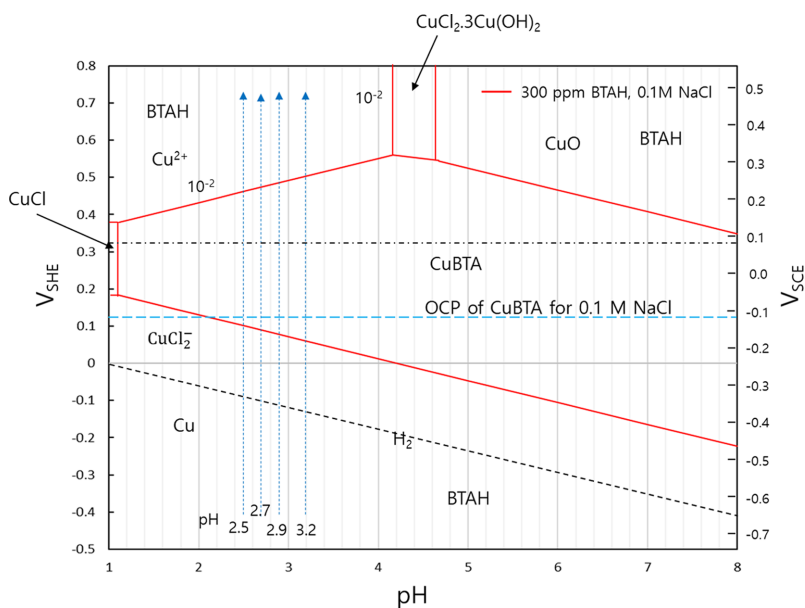


**Fig. 2. Pourbaix diagram for Cu-Cl-BTAH-H<sub>2</sub>O system in the presence of 0.1 M NaCl and 10<sup>-2</sup> M Cu<sup>2+</sup>**

regions in the Pourbaix diagram does not depend on the NaCl concentration, because there is no  $[Cl^-]$  term included in equation (1a) and (1b) for the equilibrium between CuBTA and Cu.

The horizontal black dashed dot lines at  $0.437 V_{SCE}$  and  $0.326 V_{SCE}$  for 1 M NaCl solution (Fig. 1) and the 0.1 M NaCl (Fig. 2), respectively, separates the areas dominated by aqueous species of  $Cu^{2+}$  and  $CuCl_2^-$ . The black dash line labeled  $H_2$  is the line for hydrogen electrode at one atmosphere. The blue vertical dotted arrows in Fig. 1 and Fig. 2 indicate the potential increase at the pH values of the test solutions during the potentiodynamic polarization tests.

The green, red, and blue solid lines in Fig. 1 for the 1 M NaCl solution define the stable regions of the solid phases in equilibrium with 100, 300, and 600 ppm BTAH, respectively when the activity of  $Cu^{2+}$  is  $10^{-2}$ . The CuBTA region becomes wider with increasing BTAH concentration. The upper and lower horizontal boundaries of the CuCl region are located at 0.13 and  $0.44 V_{SHE}$ , respectively. The vertical line separating the CuCl region from the CuBTA region shifts to lower pH values as the BTAH concentration increases, and it is pH 2.06 for 300 ppm BTAH.

The red solid lines in Fig. 2 for the 0.1 M NaCl solution define the stable regions of the solid phases in equilibrium with 300 ppm BTAH when the activity of  $Cu^{2+}$  is  $10^{-2}$ . One noticeable difference between the Pourbaix diagram for the BTAH containing 0.1 M NaCl solution and that for the BTAH containing 1 M NaCl solution is that CuCl region shrinks to the lower pH side for the 0.1 M NaCl solution. The boundary between the

CuCl and CuBTA regions is at pH 1.11. The  $CuCl_2 \cdot 3Cu(OH)_3$  region also shrinks as the NaCl concentration becomes smaller.

### 3.2 Polarization behavior of copper in 1 M NaCl solutions with BTAH of different concentrations at various pH values

Fig. 3 shows the polarization curves of the BTAH-free 1 M NaCl solutions at four different pH values of 5.1, 3.9, 3.3 and 3.1, together with that of tap water at pH 7.4. The open circuit potential (OCP), corrosion current density ( $I_{corr}$ ), and pitting corrosion potential ( $E_p$ ) obtained from the polarization curves of these solutions and the solutions containing BTAH are summarized in Table 2.  $E_p$  of  $0.08 V_{SCE}$  denoted by **p** is observed in the anodic polarization curve of the tap water. This pitting potential should be due to breakdown of the thin  $Cu_2O$  layer naturally formed on the copper electrode. On the other hand, there is no pitting potential observed in the curves of the BTAH-free NaCl solutions, probably due to

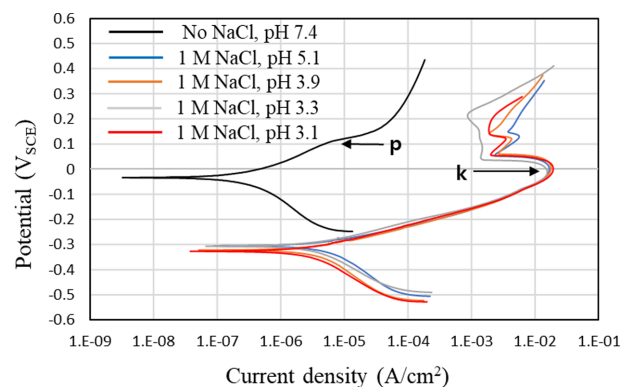


Fig. 3. Polarization behavior of Cu in BTAH-free 1 M NaCl solutions at various pH and a tap water

Table 2. Electrochemical parameters obtained from the potentiodynamic polarization tests of copper in the BTAH-added and BTAH-free 1 M NaCl solutions

pH	0 ppm BTAH			100 ppm BTAH			300 ppm BTAH			600 ppm BTAH		
	OCP ( $V_{SCE}$ )	$I_{corr}$ ( $nA/cm^2$ )	$E_p$ ( $V_{SCE}$ )	OCP ( $V_{SCE}$ )	$I_{corr}$ ( $nA/cm^2$ )	$E_p$ ( $V_{SCE}$ )	OCP ( $V_{SCE}$ )	$I_{corr}$ ( $nA/cm^2$ )	$E_p$ ( $V_{SCE}$ )	OCP ( $V_{SCE}$ )	$I_{corr}$ ( $nA/cm^2$ )	$E_p$ ( $V_{SCE}$ )
7.4 <sup>1)</sup>	-0.03	83	0.08									
5.1	-0.30	1,833	x	-0.21	143	0.22	-0.23	198	0.32	-0.21	369	0.31
3.9	-0.32	1,296	x	-0.31	487	x	-0.21	310	0.30	-0.21	274	0.41
3.3	-0.31	1,327	x	-0.30	763	x	-0.32	430	x	-0.21	121	0.35
3.1	-0.33	991	x	-0.31	1,144	x	-0.30	1,464	x	-0.32	473	x

<sup>1)</sup> Tap water of pH 7.4 with no NaCl added

<sup>2)</sup> 'x' indicates that a pitting potential is not observed

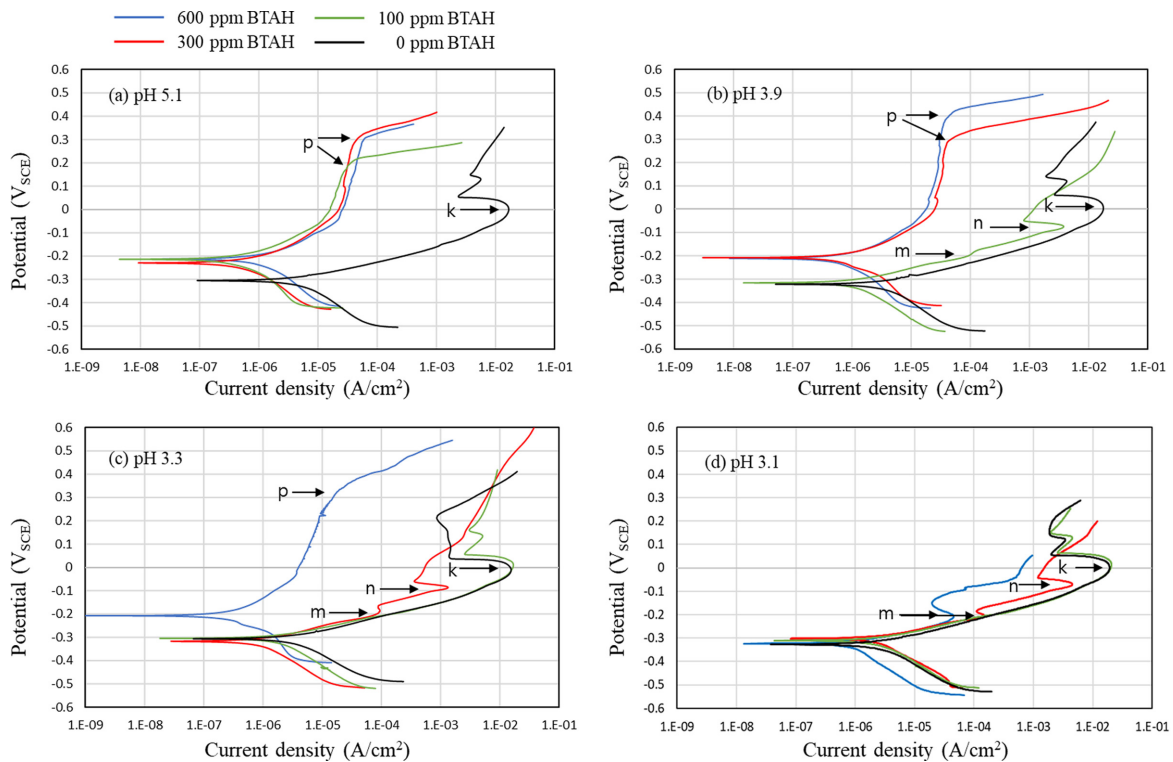


Fig. 4. Polarization behavior of Cu in BTAH-added and BTAH-free 1 M NaCl solutions at various pH

dissolution of the thin  $\text{Cu}_2\text{O}$  layer in the NaCl solutions. The polarization curves (especially anodic polarization curves) of all the BTAH-free NaCl solutions look almost the same, shifted to a much more active region with the OCP of  $-0.30$  to  $-0.33 V_{\text{SCE}}$  than the tap water with the OCP of  $-0.03 V_{\text{SCE}}$ . Resultantly,  $I_{\text{corr}}$  of the BTAH-free NaCl solutions are more than ten times bigger than the tap water. They show a typical Tafel behavior (linear increase of potential with increasing log (current density)). This result is the same as the other published result [18], and it could be expected because the dissolution equations of equation (12a) and (12b) do not have an ‘ $\text{H}^+$ ’ term [18]. Current peaks denoted by **k** are observed at around  $0 V_{\text{SCE}}$ . The **k** peaks might be due to oxidation of the copper electrode surface by chloride to form  $\text{CuCl}$  via equation (8a) and (8b) in Table 1. The potential at the **k** peaks is  $0.12 V$  higher than the equilibrium potential of  $-0.116 V_{\text{SCE}}$  ( $= 0.126 V_{\text{SHE}}$ ) determined by equation (8b), probably due to the broad potential range of this oxidation process occurring.



$$E = 0.224 + 0.0591 \log \left\{ \frac{[\text{CuCl}_2^-]}{[\text{Cl}^-]^2} \right\}, V_{\text{SHE}} \quad (12b)$$

Fig. 4a - d show the polarization behavior of copper electrodes in 1 M NaCl solutions containing 100, 300, or 600 ppm BTAH at different pH values of 5.1, 3.9, 3.3, and 3.1, respectively. The polarization behavior of the BTAH-added NaCl solution depends strongly on the BTAH concentration and the pH value. The OCP of around  $-0.21 V_{\text{SCE}}$  is observed for the following combinations of the BTAH concentration and pH in the 1 M NaCl solutions: (100, 300 or 600 ppm BTAH) and pH 5.1; (300 or 600 ppm BTAH) and pH 3.9; and 600 ppm BTAH and pH 3.3 (see Fig. 4 and Table 2). When the OCP is around  $-0.21 V_{\text{SCE}}$ , the anodic polarization curve undergoes a parabolic increase of potential with increasing log (current density) (see Fig. 4a, b and c). This polarization behavior indicates that a passive  $\text{CuBTA}$  layer was formed on the copper surface while being immersed for 5 hours before the polarization test. (Usually, the OCP keeps increasing for about 2 hours and then remains almost constant for about 3 hours.)  $E_p$  denoted by **p** are observed for these cases. This pitting potential should be due to breakdown of the combination of the  $\text{CuBTA}$  layer and the naturally formed thin  $\text{Cu}_2\text{O}$  layer. It increases slightly with increasing BTAH concentration (Fig. 5), which is

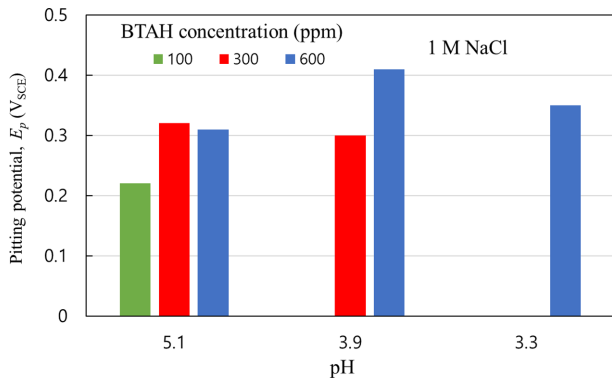


**Fig. 5. Pitting potential ( $E_p$ ) of Cu in BTAAH-added and BTAAH-free 1 M NaCl solutions at various pH**

probably due to increasing CuBTA layer thickness with increasing BTAAH concentration.

The OCP of around  $-0.31 V_{SCE}$  is observed for the following combinations of the BTAAH concentration and pH in the 1 M NaCl solutions: 100 ppm BTAAH and pH 3.9; (100 or 300) ppm BTAAH and pH 3.3; (100, 300, or 600 ppm) BTAAH and pH 3.1. When the OCP of the BTAAH-added NaCl solutions is about  $-0.31 V_{SCE}$  (see Fig. 4b, c and d), the anodic polarization curve shows almost the same linear relationship between potential and log (current density) as the BTAAH-free NaCl solutions until the potential reaches about  $-0.2 V_{SCE}$  at which the peaks denoted by **m** appear. Appearance of these **m** peaks of  $1\sim 10 \times 10^{-5} A/cm^2$  magnitude indicates that the CuBTA layer begins to form on the copper electrode surface when the potential reaches this value. However, judged by the small magnitude of the **m** peaks, these CuBTA layers are not as thick as those formed during immersion in the BTAAH solutions. Tromans and Sun [18] also observed the same current peaks of  $\sim 2.5 \times 10^{-5} A/cm^2$  at about  $-0.2 V_{SCE}$ . They thought that this current peak is due to fast precipitation of CuBTA by the reaction of equation (13a) and (13b) onto the copper surface, derived by the high enough activity of  $CuCl_2^-$  which increases with increasing potential (see equation (12a) and (12b)) [23]. The peaks denoted by **n** are found at about  $-0.1 V_{SCE}$  for pH 3.9, 3.3 and 3.1 when the OCP is around  $-0.31 V_{SCE}$ . These peaks might be due to oxidation of Cu to CuCl by  $Cl^-$  via equation (8a) and (8b).



$$k = \frac{[H^+][Cl^-]^2}{[CuCl_2^-][BTAAH]} = 1.54 \times 10^2 \quad (13b)$$

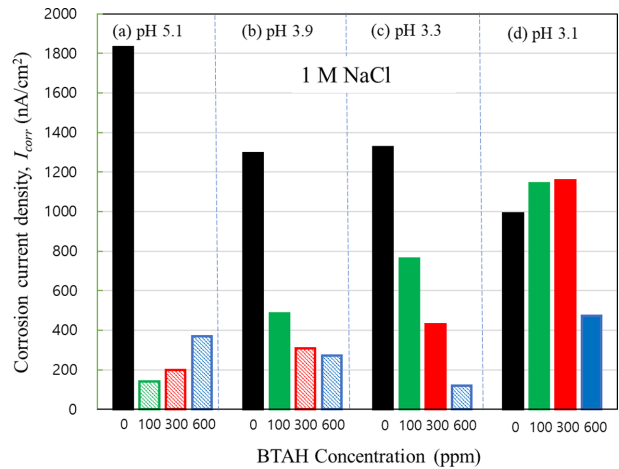


**Fig. 6. Corrosion current density ( $I_{corr}$ ) of Cu in BTAAH-added and BTAAH-free 1 M NaCl solutions at various pH**

Fig. 6 compares  $I_{corr}$  for the solutions with different BTAAH concentrations at different pH.  $I_{corr}$  was plotted as a bar with stripes when the OCP was around  $-0.21 V_{SCE}$ , while it was plotted as a solid bar when the OCP was around  $-0.31 V_{SCE}$ .  $I_{corr}$  for the BTAAH-added solutions with the OCP of  $-0.21 V_{SCE}$  are much smaller than those for the solutions with the OCP of  $-0.31 V_{SCE}$ , meaning that the corrosion rate is reduced significantly if the CuBTA layer is formed. The advantage of the passivity of the CuBTA layer becomes amplified if the potential is increased, for example, to  $-0.1 V_{SCE}$  at which the anodic current is reduced to about 1/500 of that for the solution in which the CuBTA layer is not formed.

Cathodic polarization behavior of copper in an aqueous solution should be determined by hydrogen reduction when the potential is below the hydrogen reduction line, while it is determined by reduction of trace oxygen just below the OCP. When the OCP is around  $-0.31 V_{SCE}$  and therefore CuBTA is not formed, the cathodic polarization curve shifts slightly to a lower current region as the BTAAH concentration increases (see Fig. 4), resulting in a lower corrosion current density (see Fig. 6). This is probably because a denser BTAAH film is adsorbed to the copper electrode surface without forming a CuBTA layer, slowing down the cathodic reaction of hydrogen or oxygen reduction. Yao et al. [26] also concluded using their potential-dependent Raman study that BTAAH adsorbs in the form of neutral BTAAH molecules on the Cu surface to form an adsorption layer in the negative potential region and in the form of deprotonated BTA $^-$

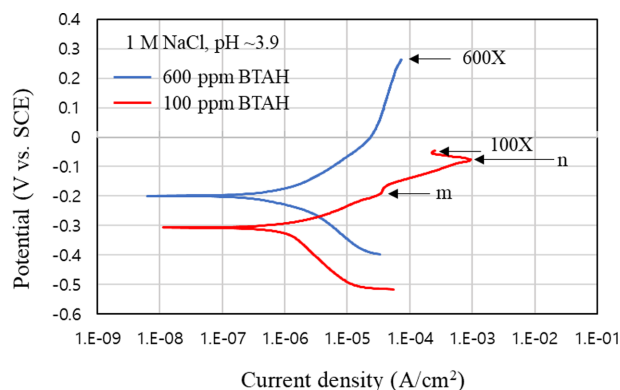


**Fig. 7. Potentiodynamic polarization curves of Cu in 100 and 600 ppm BTAH-added 1 M NaCl solutions at pH around 3.9 for specimens of XPS analysis**

ion to form a compact polymer film  $[\text{Cu}(\text{BTA})]_n$  in the positive potential region. On the other hand, when the CuBTA layer is not formed, the anodic polarization curve does not depend on the BTAH concentration in the potential range between  $-0.3 V_{\text{SCE}}$  and  $-0.2 V_{\text{SCE}}$  which is the potential of the **m** peak (see Fig. 4c and d). Because of this phenomenon, even in the case that the CuBTA layer is not formed, the higher BTAH concentration would lead to the smaller  $I_{\text{corr}}$ .

To confirm by XPS analysis whether the CuBTA layer is really formed when the OCP is around  $-0.21 V_{\text{SCE}}$ , the following experiments were performed. Firstly, a copper specimen was immersed for 5 hours in 1 M NaCl solution at pH around 3.9 containing 100 or 600 ppm BTAH. The specimens were named as 100X and 600X according to their BTAH concentrations in ppm with the letter ‘X’ attached at the end. The voltage on the specimen was increased during the potentiodynamic polarization test up to the point indicated by the specimen’s name in Fig. 7. After finishing the polarization tests, the specimens were analyzed by XPS. Fig. 8a and b are the XPS survey spectra of the specimens 600X and 100X, respectively. The carbon peak at 285 eV (C1s) seems due to both contaminant carbon and carbon present in BTAH [27]. The N1s peak at 400 eV is clearly seen for the specimen 600X, indicating that a thin CuBTA layer was formed on the specimen 600X with an OCP of  $-0.20 V_{\text{SCE}}$ . On the other hand, the N1s peak is barely seen for the specimen 100X with an OCP of  $-0.31 V_{\text{SCE}}$ , indicating that almost no CuBTA layer was formed while the specimen was immersed in the solution, except when the voltage was

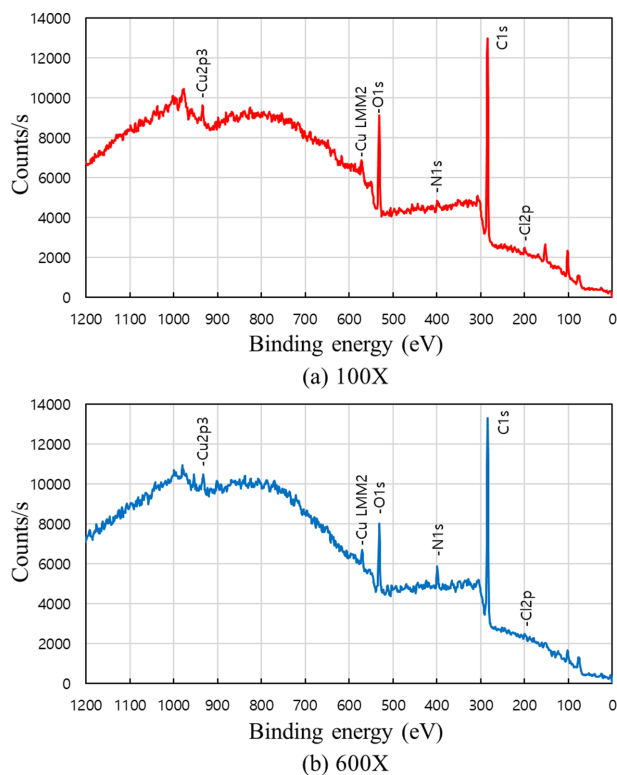


**Fig. 8. XPS survey spectra of the specimens (a) 100X and (b) 600X (see Fig.7 for the specimens)**

passing through the small **m** peak (see Fig. 7). In the XPS spectra of the specimen 100X, a small Cl2p appears, indicating that CuCl was formed through the reaction of equation (8a) and (8b) occurring at around the **n** peak. The above results show that if the CuBTA layer is formed in a 1 M NaCl solution with BTAH added, the OCP should have a value of around  $-0.21 V_{\text{SCE}}$ .

The strong dependence of the CuBTA layer formation on both BTAH concentration and pH can be discussed further referring to the Pourbaix diagram of 1 M NaCl solution (Fig. 1). The boundary between the CuBTA and Cu regions in the Pourbaix diagram at pH 5.1 is located lower than the OCP ( $-0.21 V_{\text{SCE}}$ ) for all of the 100, 300, and 600 ppm BTAH solutions. This means that the CuBTA layer formed on the copper surface in these solutions becomes thermodynamically stable as confirmed by this study (Fig. 4a). At pH 3.9, the boundaries between the CuBTA and Cu regions for the 300 and 600 ppm BTAH solutions are located below  $-0.21 V_{\text{SCE}}$ , indicating that the CuBTA layer formed becomes stable (Fig. 4b). On the other hand, the boundary between the CuBTA and Cu regions for the 100 ppm

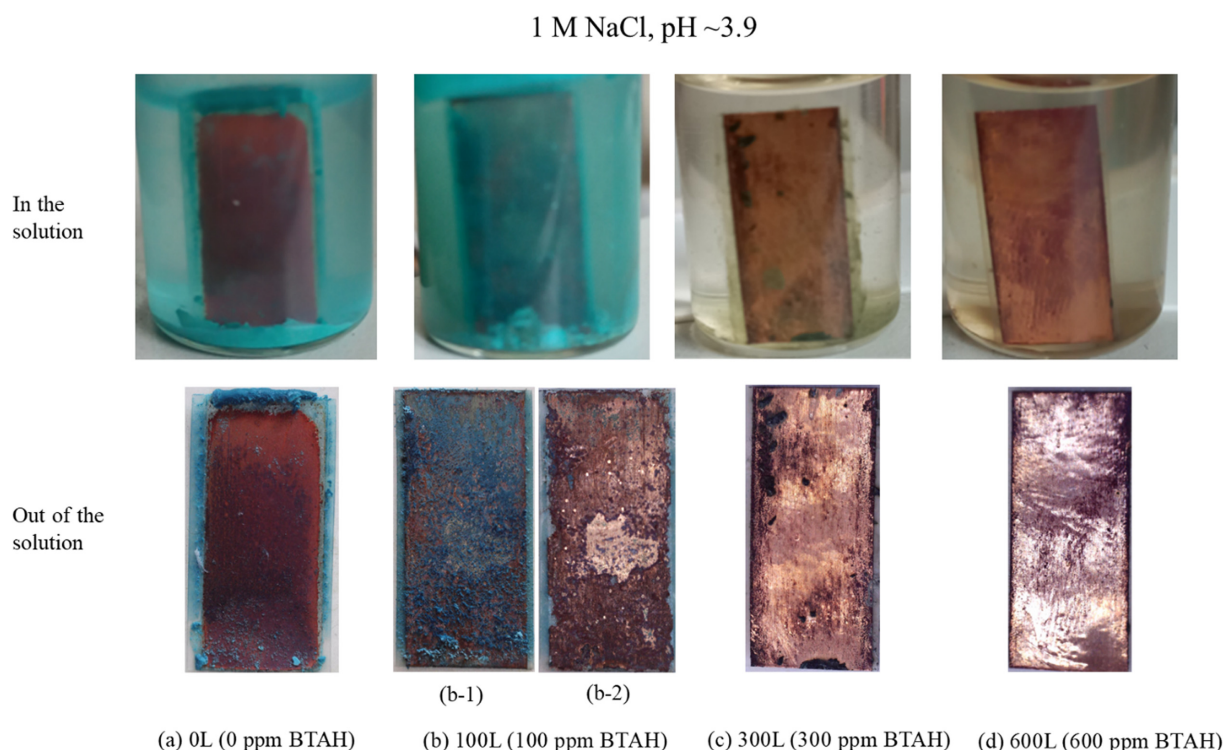


**Fig. 9. Copper tape specimens immersed for 2.3 years in 1 M NaCl solutions at pH around 3.9 with BTAAH of 0 to 600 ppm added**

BTAH solution is located almost at  $-0.21 V_{SCE}$ , suggesting that the CuBTA layer formed on the copper surface in the 100 ppm BTAH solution may not be thermodynamically stable (Fig. 4b). In this case, only when the potential is increased above  $-0.21 V_{SCE}$ , the CuBTA layer is formed as manifested by the appearance of the peak *m* (Fig. 4b). At pH 3.3, the boundary between the CuBTA and Cu regions nearly touches the OCP line of CuBTA for 1 M NaCl at  $-0.21 V_{SCE}$  for the 600 ppm BTAH solution, suggesting that the CuBTA layer could be thermodynamically stable only in this solution (Fig. 4c). At pH 3.1, the boundaries between the CuBTA and Cu regions in the Pourbaix diagram for all three solutions are located well above  $-0.21 V_{SCE}$ , making the CuBTA layer unstable (Fig. 4d). To form a stable CuBTA layer at pH lower than 3.3, the BTAH concentration should be higher than 600 ppm.

### 3.3 Analysis of the copper specimens immersed for 2.3 years in 1 M NaCl solutions at pH 3.9 with different BTAH concentrations

To investigate the BTAH concentration dependence of the corrosion inhibition efficiency qualitatively, copper tape specimens bonded on PVC sheets were immersed

**Table 3. Surface of composition of the specimens 100L and 600L measured by XPS (at.%)**

Element	Specimen	
	100L	600L
C1s	62.57	65.40
N1s	9.34	19.98
O1s	18.10	9.67
Cl2p	1.99	0.44
Cu2p3	8.01	4.51

for 2.3 years in the 1 M NaCl solutions at pH around 3.9 added with BTAH of 0, 100, 300, and 600 ppm (see top photos of Fig. 9). The bottom photos of Fig. 9 show the specimens taken out from the solutions. The specimens were named according to their BTAH concentrations in ppm with the letter 'L' attached at the end. Blue-green corrosion product powders, which look like copper chloride dihydrate ( $CuCl_2 \cdot 2H_2O$ ), are settled at the bottom of the bottles of the 0 and 100 ppm BTAH solutions. Some corners and edges of the specimens 0L and 100L were dissolved away by corrosion. The color of the specimen 0L turned into dark red. Dark green corrosion product particles are deposited on the specimen 100L (Fig. 9b-1), while it

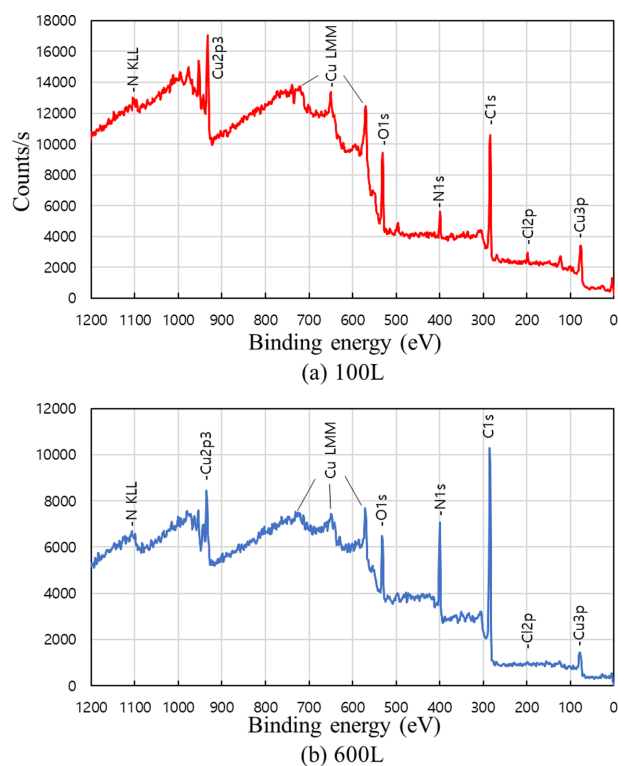


**Fig. 10. XPS survey spectra of the specimens (a) 100L and (b) 600L (see Fig. 9 for the specimens)**

became dark brown when the particles were removed using a scotch tape (see Fig. 9b-2) There are some regions, especially at the center of the specimen 100L, which maintain the color of original copper specimen.

The specimen 300L has a small amount of dark brown corrosion products at the top left and the bottom of the specimen surface. There are no blue-green corrosion product powders settled in the bottle. The specimen 600L has almost no corrosion products observed over the entire surface with maintaining its original brightness of the copper specimen, meaning that almost no corrosion has occurred during this period of time.

The surface concentration of the specimens 100L and 600L was analyzed by XPS. Fig. 10a and b show the survey spectra of these two specimens. Most of the peaks for these specimens are better defined than those of the specimens 100X and 600X, probably because of much longer immersion time for these specimens. The specimen 600L has a stronger N1s peak than the specimen 100L. Actually, the surface of the specimen 600L has 20 at.% N1s, while the N1s composition of the specimen 100L is 9.34 at.% (see Table 3). The reason why the specimen

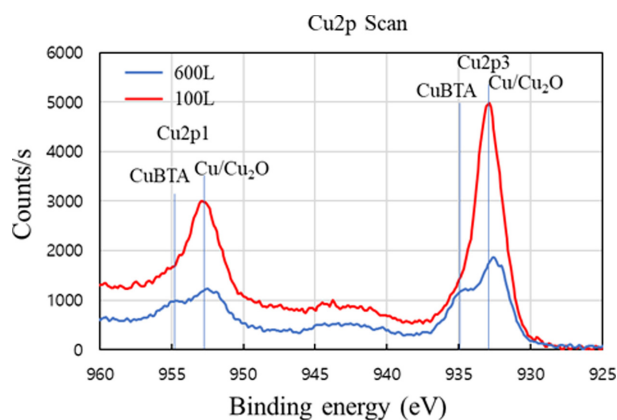


**Fig. 11. Cu2p spectra of the specimens (a) 100L and (b) 600L (see Fig.9 for the specimens)**

100L also has this high concentration of nitrogen is probably because this specimen contains a seemingly intact bright region at the center (see Fig. 9b-2). The specimen 100L shows high Cl2p concentration of 1.99 at.%, while the specimen 600L has almost no Cl2p concentration, which is another evidence that the specimen 600L underwent almost no corrosion.

The Cu2p peaks were investigated in detail to study the structure of the corrosion inhibition layer (Fig. 11). The Cu2p3 spectra consist of two peaks at 933 and 935 eV. The peaks at 933 eV are due to Cu and Cu<sub>2</sub>O, while the peaks at 935 eV are believed due to CuBTA [11,28]. For the specimen 100L, the CuBTA peak is much smaller than the Cu/Cu<sub>2</sub>O peak. On the other hand, for the specimen 600L, the CuBTA peak height is comparable to that of the Cu/Cu<sub>2</sub>O peak. The similarly shaped but smaller peaks of Cu/Cu<sub>2</sub>O and CuBTA are observed in the Cu2p1 spectra as well. These results and the photos of the specimens in Fig. 9 indicate that the CuBTA layer was formed well in the specimen 600L, while the CuBTA layer was formed in the specimen 100L as well, but either incompletely or unevenly.

The above results support the conclusion obtained in the section 3.2 that only when the (pH, OCP) is located well in the CuBTA region of the Pourbaix diagram, a stable corrosion inhibiting CuBTA layer could be formed.

### 3.4 Polarization behavior of copper in 0.1 M NaCl solutions with 300 ppm BTAH at various pH values

Fig. 12 shows the polarization behavior of the copper electrode in 300 ppm BTAH-added 0.1 M NaCl solutions

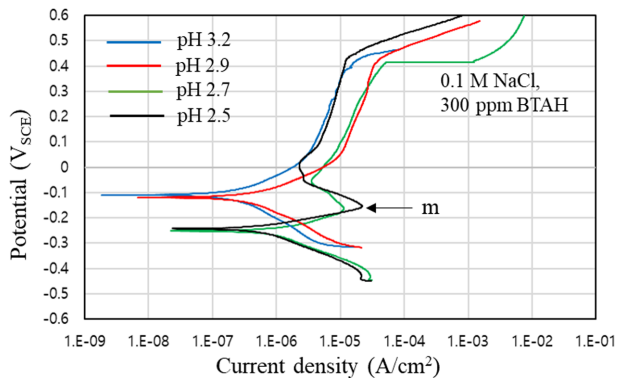


Fig. 12. Polarization behavior of Cu in 300 ppm BTAH-added 0.1 M NaCl solutions at various pH

Table 4. Electrochemical parameters obtained from the potentiodynamic polarization tests of copper in the 300 ppm BTAH-added 0.1 M NaCl solutions at different pH values

pH	OCP (V <sub>SCE</sub> )	I <sub>corr</sub> (nA/cm <sup>2</sup> )	E <sub>p</sub> (V <sub>SCE</sub> )
3.2	-0.11	83	0.42
2.9	-0.12	152	0.41
2.7	-0.25	544	0.40
2.5	-0.24	308	0.43

at various pH values of 2.5 to 3.2. The electrochemical parameters obtained from these polarization tests are given in Table 4. The OCP is around -0.12 V<sub>SCE</sub> at pH equal to or higher than 2.9, indicative of formation of a CuBTA layer. On the other hand, it is about -0.25 V<sub>SCE</sub> at pH equal or lower than 2.7, showing that the CuBTA layer is not formed at these low pH values. The current peaks denoted by **m** are observed at around -0.16 V<sub>SCE</sub> in the anodic polarization curves of the solutions at pH 2.7 and 2.5. After formation of a CuBTA layer was completed at about 0 V<sub>SCE</sub>, the anodic polarization curves of these solutions begin to follow the curve for the solution either at pH 3.2 or pH 2.9. Unlike the polarization curves for the 1 M NaCl solutions, there is no **n** peaks observed which is related to the formation of CuCl. This may be because the surface of copper electrode becomes so completely covered with the sound CuBTA layer during the period of potential increase that copper cannot be oxidized to CuCl via equation (8a) and (8b). Fig. 13 shows the corrosion current density of copper in the 0.1 M NaCl solution with 300 ppm BTAH at different pH values. When the CuBTA layer was formed on the copper surface,

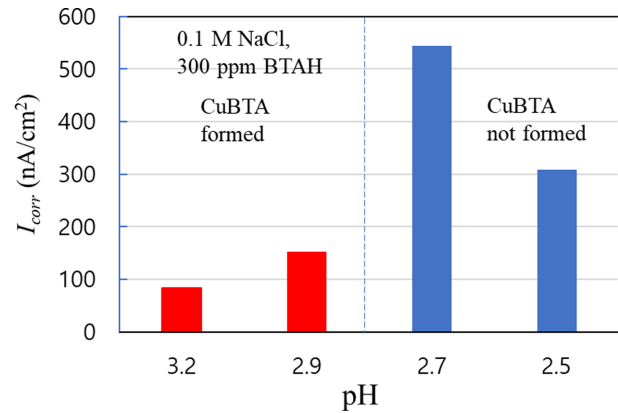


Fig. 13. Corrosion current density ( $I_{corr}$ ) of Cu in 300 ppm BTAH-added 0.1 M NaCl solutions at various pH

the corrosion current density,  $I_{corr}$  was more than two times lower than those obtained when the CuBTA layer could not be formed.

The OCP of -0.12 V<sub>SCE</sub> for a stable CuBTA layer in the 0.1 M NaCl solution is higher than that of -0.21 V<sub>SCE</sub> for the 1 M NaCl solutions. The higher OCP in the 0.1 M NaCl solution allowed the CuBTA layer to be formed at lower pH values of 3.2 and 2.9 in the 0.1 M NaCl solutions than those in the 1 M NaCl solutions. At pH 3.2 and 2.9, the boundaries between the CuBTA and Cu regions in the Pourbaix diagram of the 0.1 M NaCl solution (Fig. 2) are located well below the OCP of -0.12 V<sub>SCE</sub>, indicating that the CuBTA layer formed becomes stable. However, the boundaries between the OCP and Cu regions at pH 2.7 and 2.5, where the CuBTA layer was not formed initially, are still located below the OCP of -0.12 V<sub>SCE</sub>, even though the difference between the OCP and the boundary was reduced proportionally with decreasing pH. Therefore, for the CuBTA layer to be formed safely on the copper surface in the 0.1 M NaCl solution at a particular pH value, BTAH concentration should be high enough so that the boundary between the CuBTA and Cu regions at that pH value in the Pourbaix diagram is located at least 0.05 V below the OCP.

### 3.5 Polarization behavior of copper in the 300 ppm BTAH solutions with various NaCl concentrations

The polarization behavior of copper was tested in the 300 ppm BTAH solutions at around pH 4.2 with various NaCl concentrations from 0.01 M to 1 M (Fig. 14). The electrochemical parameters obtained from the tests are given in Table 5. The anodic polarization curves of all

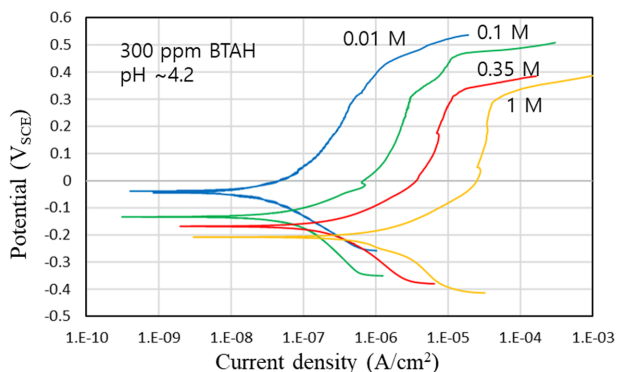


Fig. 14. Polarization behavior of Cu in 300 ppm BTAH-added solutions with different NaCl concentrations at pH 4.2

Table 5. Electrochemical parameters obtained from the potentiodynamic polarization tests of copper in the 300 ppm BTAH solutions with various NaCl concentrations at around pH 4.2

NaCl conc (M)	[Cl <sup>-</sup> ] activity	OCP (V <sub>SCE</sub> )	I <sub>corr</sub> (nA/cm <sup>2</sup> )	E <sub>p</sub> (V <sub>SCE</sub> )
0.01	0.0093	-0.046	7	0.42
0.10	0.078	-0.132	21	0.30
0.35	0.249	-0.168	76	0.32
1	0.67	-0.207	310	0.30

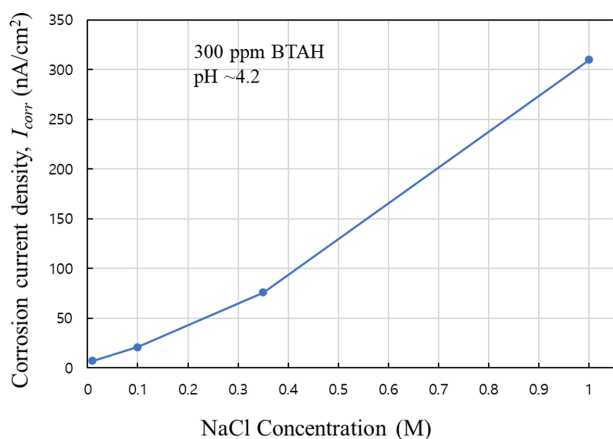


Fig. 15. Corrosion current density ( $I_{corr}$ ) of Cu vs. NaCl concentration in the 300 ppm BTAH solutions at pH around 4.2

the four solutions show a parabolic increase of potential with increasing log (current density), indicative of CuBTA formation. The polarization curve was shifted to a more active region of higher currents and lower potentials as the NaCl concentration was increased. Fig. 15 shows that  $I_{corr}$  increases almost linearly with increasing NaCl concentration. Both the anodic and cathodic currents

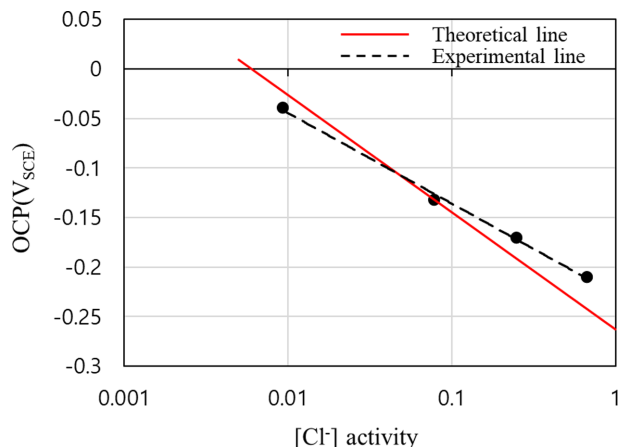


Fig. 16. Dependence of the OCP for CuBTA formation on the chloride activity

increase with increasing NaCl concentration.

Fig. 16 shows the dependence of the OCP on the [Cl<sup>-</sup>] activity (= NaCl mole concentration times its activity coefficient). As the black dotted trend line shows, the OCP decreases with increasing [Cl<sup>-</sup>] activity with a logarithmic dependency (equation (14a)). This dependency could be expressed in terms of the NaCl mole concentration, [NaCl] by equation (14b). The OCP for the stable CuBTA formation is almost the same as the potential for the **m** peaks shown in Fig. 4 for the 1 M NaCl solutions and Fig. 12 for the 0.1 M NaCl solutions. This might mean that the OCP is determined by the potential at which the activity of [CuCl<sub>2</sub><sup>-</sup>] reaches a high enough value for fast precipitation of CuBTA, as Tromans [23] argued for the **m** peaks. Assuming that the [CuCl<sub>2</sub><sup>-</sup>] activity for precipitation of CuBTA is a constant independent of NaCl concentration, a relationship between the [Cl<sup>-</sup>] activity and the OCP could be obtained by substituting a specific [Cl<sup>-</sup>] activity for [Cl<sup>-</sup>] and its corresponding OCP for E in Eq (12b). By substituting 0.078 for [Cl<sup>-</sup>] of 0.1 M NaCl solution and the observed OCP of -0.132 V<sub>SCE</sub>, a theoretical equation of equation (15) could be obtained. The theoretical line of equation (15) was drawn as a red line in Fig. 15 together with the black dashed experimental line. A slight difference observed between these two curves is probably due to a nonnegligible dependence of [CuCl<sub>2</sub><sup>-</sup>] for CuBTA precipitation on the [Cl<sup>-</sup>] activity.

$$\text{Experimental OCP} = -0.0921 \log[\text{Cl}^-] - 0.227, V_{\text{SCE}} \quad (14a)$$

$$= -0.0852 \log[\text{NaCl}] - 0.211, V_{\text{SCE}} \quad (14b)$$

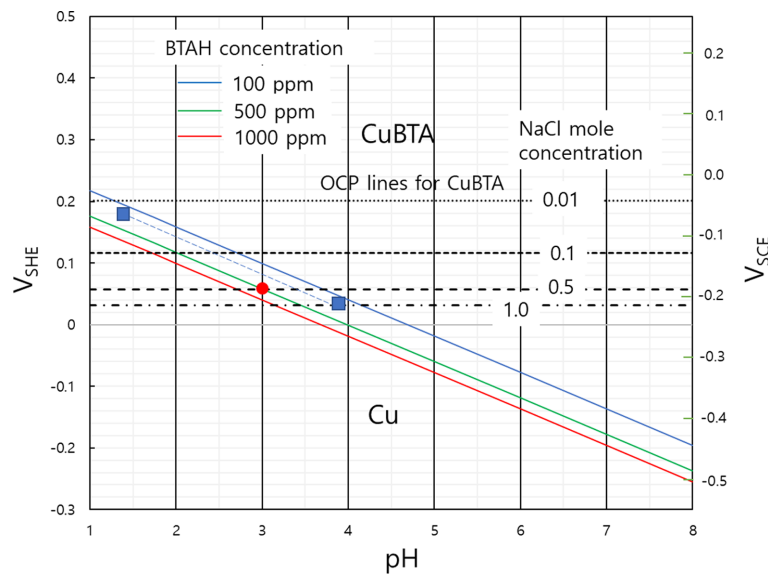


**Fig. 17. Determination of the BTAH concentration needed to form the CuBTA layer on copper in the acidic NaCl solution by using the Pourbaix diagram of Cu-Cl-BTAH-H<sub>2</sub>O system**

Theoretical OCP

$$= -0.1182 \log[\text{Cl}^-] - 0.263, V_{\text{SCE}} \quad (15)$$

Using the above results, the BTAH concentration needed to form a stable CuBTA at a combination of the NaCl concentration and pH can be determined from the Pourbaix diagram. Firstly, the OCP values for the stable CuBTA at different NaCl concentrations are obtained by equation (14a), and the corresponding OCP lines are drawn on the Pourbaix diagram which shows only the boundaries between the CuBTA and Cu phases for many different BTA concentrations (see Fig. 17). Then, the CuBTA/Cu boundary line passing through the junction between the pH line for the given pH value and the OCP line for the given NaCl concentration becomes the line for the minimum BTAH concentration needed to form a stable CuBTA. For example, the minimum BTAH concentration needed to form the stable CuBTA layer on copper in a solution of 0.5 M NaCl and pH 3 is 500 ppm, as indicated by a red dot in Fig. 17.

### 3.6 CuBTA layer formation inside a corrosion pit and the water chemistry inside the corrosion pit

It would be interesting to see if the CuBTA layer is formed inside the corrosion pit in the sprinkler copper tube when a sprinkler system of an apartment is filled with BTAH solution. The authors have used BTAH in

order to reduce the water leakage in sprinkler copper tubes which is caused by pitting corrosion. They filled the copper tubes of more than 300 sprinkler systems in a 10 year old apartment complex with 400 ppm BTAH solution. The details of how to fill the sprinkler copper tubes with the BTAH solution is described in the authors' other paper [10]. The BTAH concentration inside the copper tubes was expected to be about 320 ppm because some water was remaining in the tubes before filling the BTAH solution. There was only one water leakage for 1 year period in this apartment complex, which occurred 5 months after filling the BTAH solution. This corresponds to more than 90% reduction in the water leakage frequency. The leaked copper tube was collected and analyzed using EDS and XPS. The followings are the results.

Fig. 18a and b show the photos of a corrosion pit found in the leaked copper tube. Fig. 18a is the photo after the black colored cupric oxide (CuO) and green colored malachite (Cu<sub>2</sub>CO<sub>3</sub>(OH)<sub>2</sub>) layers were removed, while Fig. 18b is the photo of the corrosion pit bottom taken after brown colored cuprous oxide (Cu<sub>2</sub>O) particles were scraped off from the corrosion pit. Fig. 18c shows the diffusion path of BTAH as well as the cross-section of the corrosion pit. The composition at the positions D and F in Fig. 18a and b were measured by EDS and XPS, respectively, and their spectra are

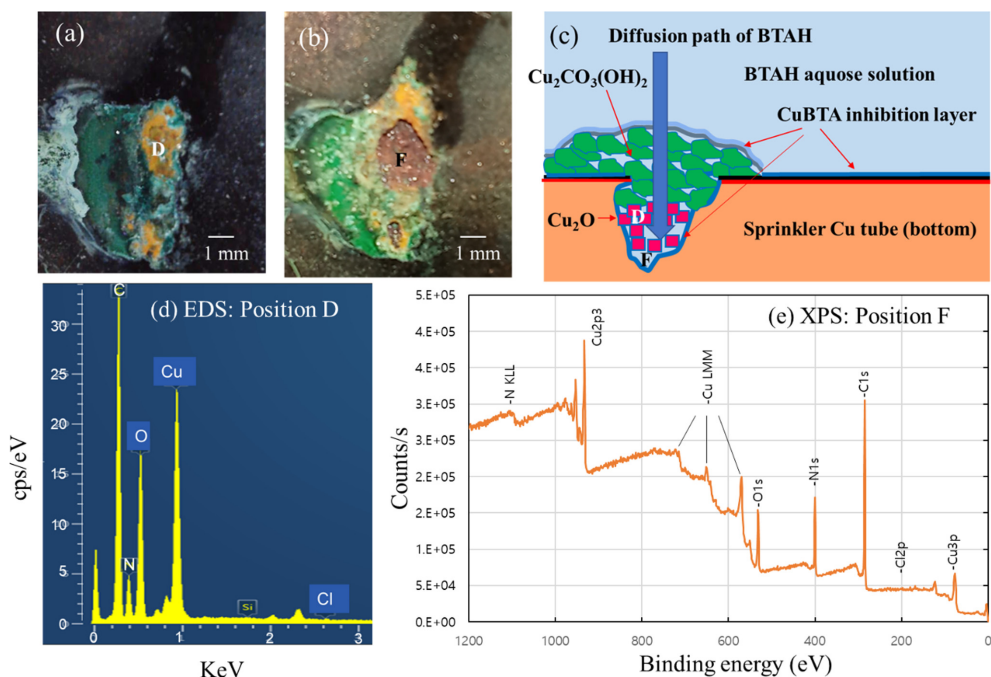


Fig. 18 (a) corrosion pit found in a sprinkler copper tube filled with 320 ppm BTAH, (b) the same corrosion pit with  $\text{Cu}_2\text{O}$  particles removed, (c) schematic diagram showing the cross-section of a corrosion pit and the diffusion path of BTAH through the corrosion pit, (d) EDS analysis result of the position D, and (e) XPS survey spectrum of the position F

Table 6. Composition of the positions D and F of a corrosion pit measured by EDS and XPS, respectively (at.%). This corrosion pit was found in a leaked sprinkler copper tube treated by 320 ppm BTAH solution

Element \ Position	D (EDS)	F (XPS)
C (C1s)	54.95	54.55
N (N1s)	14.86	18.61
O (O1s)	20.70	15.79
Cl (Cl2p)	0.09	1.14
Cu (Cu2p3)	9.38	10.01

shown in Fig. 18d and e. The EDS and XPS spectra are quite similar in shape to each other. Actually, the composition at the position D obtained by EDS is almost the same as the composition at position F obtained by XPS (see Table 6). Both positions have high N concentration and low Cl concentration. This means that  $\text{Cu}_2\text{O}$  particles in the corrosion pit and the corrosion pit bottom are coated well with CuBTA. The nitrogen (N) composition at the position F is also similar to that of the specimen 600L which showed almost no corrosion, meaning again that a sound CuBTA layer was formed at the bottom of the corrosion pit.

The Cu2p peaks were investigated for this corrosion pit (Fig. 19). The Cu2p3 spectra consist of two peaks at 932.5 and 934.5 eV which are almost the same as those for the specimen 600L. However, the CuBTA peak height with respect the Cu/ $\text{Cu}_2\text{O}$  height is smaller than that for the specimen 600L. This might mean that the CuBTA layer formed in the corrosion pit is thinner than that formed in the specimen 600L. Similarly shaped peaks of Cu/ $\text{Cu}_2\text{O}$  and CuBTA are observed in the Cu2p1 spectra as well. The important point is that the CuBTA layer was formed well inside the corrosion pit, and it helped reduce the water leakage rate by about 90%.

It might be possible to estimate the water chemistry inside the copper corrosion pit, using the results of this study. 320 ppm BTAH solution was effective in reducing the water leakage of sprinkler copper tubes and it was confirmed that the CuBTA layer was formed well in the corrosion pit by this solution. The authors also found that 100 ppm BTAH solution was not effective in reducing the water leakage rate of sprinkler copper tubes. These two results suggest that the water chemistry inside the copper corrosion pit could be similar to that of 1 M NaCl solution at pH around 3.9 as far as the corrosion

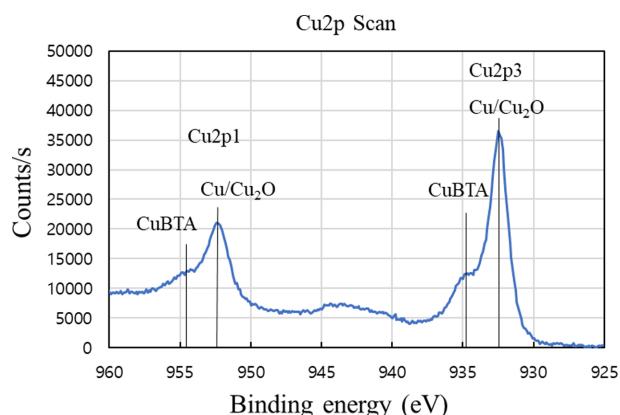


**Fig. 19** Cu2p spectra of the corrosion pit bottom of a sprinkler copper tube (position F)

inhibiting strength is concerned. However, the real water chemistry in the corrosion pit would be different from the combination of 1 M  $[\text{Cl}^-]$  and pH 3.9 because this combination may not satisfy the electrical neutrality inside a corrosion pit ( $10^4$  times higher  $[\text{Cl}^-]$  than  $[\text{H}^+]$ ). If the  $\text{Cl}^-$  concentration is equal to the  $\text{H}^+$  concentration so that the electrical neutrality condition is satisfied only by these two species, the 0.03 M  $[\text{Cl}^-]$ /pH 1.5 might become the water chemistry inside the corrosion pit. The two combinations of 1 M  $[\text{Cl}^-]$ /pH 3.9 and 0.03 M  $[\text{Cl}^-]$ /pH 1.5 are indicated in Fig. 17 as solid squares which are connected to each other by a dashed line. If the electrical neutrality condition is satisfied not only by  $[\text{Cl}^-]$  and  $[\text{H}^+]$  but also by other positive ions such as  $[\text{Cu}^{2+}]$ , the water chemistry would change to a higher  $[\text{Cl}^-]$ /higher pH combination than the 0.03 M  $[\text{Cl}^-]$ /pH 1.5 combination along the dashed line. This could be the subject of further study either by experiment or simulation.

#### 4. Conclusions

The polarization behavior of copper in BTAH-added NaCl aqueous solutions at different pH values was studied, with reference to the Pourbaix diagrams constructed for 1 M and 0.1 M NaCl solutions with different BTAH concentrations. Formation of the corrosion inhibiting CuBTA layer was studied by the potentiodynamic polarization tests and the EDS/XPS analysis. The following conclusions were obtained from this study.

The OCPs of  $-0.21 V_{\text{SCE}}$  and  $-0.12 V_{\text{SCE}}$  were obtained

for 1 M and 0.1 M NaCl solutions, respectively, when the CuBTA layer is formed on the copper electrode. These OCPs do not depend on either pH or BTAH concentration of the solutions. The OCPs are lowered to  $0.31 V_{\text{SCE}}$  and  $-0.25 V_{\text{SCE}}$  for 1 M and 0.1 M NaCl solutions, respectively, when the CuBTA layer is not formed.

It is concluded from the polarization behavior of copper in the 300 ppm BTAH solutions with various NaCl concentrations that the OCP value for the stable CuBTA layer depends on the  $[\text{Cl}^-]$  activity logarithmically.

For a stable CuBTA layer to be formed by BTAH on copper at a particular combination of the NaCl concentration and pH, a high enough BTAH concentration should be used so that the (pH, OCP) is well in the CuBTA region of the Pourbaix diagram.

BTAH concentration to obtain a stable CuBTA layer in a NaCl solution can be determined from the Pourbaix diagram of Cu- $\text{Cl}^-$ -BTAH- $\text{H}_2\text{O}$  system with the help of the OCP line for the NaCl concentration drawn on the diagram.

When the sprinkler copper tube is filled with 320 ppm BTAH solution, a corrosion inhibiting CuBTA layer can be formed inside the corrosion pit in the sprinkler copper tube, reducing the water leakage rate greatly.

The information obtained through this study could be used to estimate the water chemistry inside the corrosion pit.

#### Acknowledgment

A part of this research was supported by the Korea Land & Housing Corporation.

#### References

1. H. P. Lee, K. Nobe, Kinetics and Mechanisms of Cu Electrodeposition in Chloride Media, *Journal of The Electrochemical Society*, **133**, 2035 (1986). Doi: <https://doi.org/10.1149/1.2108335>
2. A. L. Bacarella, J. C. Griess, The Anodic Dissolution of Copper in Flowing Sodium Chloride Solutions Between 25° and 175 °C, *Journal of The Electrochemical Society*, **120**, 459 (1973). Doi: <https://doi.org/10.1149/1.2403477>
3. H. Cong, J. R. Scully, Effect of Chlorine Concentration on Natural Pitting of Copper as a Function of Water Chemistry, *Journal of The Electrochemical Society*, **157**,

- C200 (2010). Doi: <https://doi.org/10.1149/1.3337005>
4. J. C. Rushing, M. Edwards, Effect of aluminum solids and chlorine on cold water pitting of copper, *Corrosion Science*, **46**, 3069 (2004). Doi: <https://doi.org/10.1016/j.corsci.2004.05.021>
  5. H. Cong, H. T. Michels, J. R. Scully, Passivity and Pit Stability Behavior of Copper as a Function of Selected Water Chemistry Variables, *Journal of The Electrochemical Society*, **156**, C16 (2009). Doi: <https://doi.org/10.1149/1.2999351>
  6. D. A. Lytle, M. R. Schock, Pitting corrosion of copper in waters with high pH and low alkalinity, *Journal American Water Works Association*, **100**, 115 (2008). Doi: <https://doi.org/10.1002/j.1551-8833.2008.tb09586.x>
  7. D. A. Lytle, M. N. Nadagouda, A comprehensive investigation of copper pitting corrosion in a drinking water distribution system, *Corros. Sci.* **52** (2010) 1927-1938. Doi: <https://doi.org/10.1016/j.corsci.2010.02.013>
  8. Claes Taxén, Pitting corrosion of copper An equilibrium — mass transport study, 2002. <https://skb.se/upload/publications/pdf/TR-02-22.pdf> (accessed March 12, 2021).
  9. Claes Taxén, Pitting corrosion of copper Further model studies (2002).
  10. S. H. Suh, Y. Suh, S. Kim, J.-M. Yang, G. Kim, Pitting Corrosion Inhibition of Sprinkler Copper Tubes via Forming of Cu-BTA Film on the Inner Surface of Corrosion pits, *Corrosion Science and Technology*, **18**, 49 (2019). Doi: <https://doi.org/10.14773/cst.2019.18.2.39>
  11. Y. H. Lee, M. S. Hong, S. J. Ko, J. G. Kim, Effect of benzotriazole on the localized corrosion of copper covered with carbonaceous residue, *Materials*, **14**, 2722 (2021). Doi: <https://doi.org/10.3390/ma14112722>
  12. F. MANSFELD, T. SMITH, E. P. PARRY, Benzotriazole as Corrosion Inhibitor for Copper, *CORROSION*, **27**, 289 (1971). Doi: <https://doi.org/10.5006/0010-9312-27.7.289>
  13. V. Brusica, M. A. Frisch, B. N. Eldridge, F. P. Novak, F. B. Kaufman, B. M. Rush, G. S. Frankel, Copper Corrosion With and Without Inhibitors, *Journal of The Electrochemical Society*, **138**, 2253 (1991). Doi: <https://doi.org/10.1149/1.2085957>
  14. M. R. Vogt, W. Polewska, O. M. Magnussen, R. J. Behm, In Situ STM Study of (100) Cu Electrodes in Sulfuric Acid Solution in the Presence of Benzotriazole: Adsorption, Cu Corrosion, and Cu Deposition, *Journal of The Electrochemical Society*, **144**, L113 (1997). Doi: <https://doi.org/10.1149/1.1837629>
  15. G. W. Poling, Reflection infra-red studies of films formed by benzotriazole on Cu, *Corrosion Science*, **10**, 359 (1970) Doi: [https://doi.org/10.1016/S0010-938X\(70\)80026-9](https://doi.org/10.1016/S0010-938X(70)80026-9)
  16. R. WALKER, Triazole, Benzotriazole and Naphthotriazole as Corrosion Inhibitors for Copper, *CORROSION*, **31**, 97 (1975). Doi: <https://doi.org/10.5006/0010-9312-31.3.97>
  17. T. Kosec, I. Milošev, B. Pihlar, Benzotriazole as an inhibitor of brass corrosion in chloride solution, *Applied Surface Science*, **253**, 8863 (2007). Doi: <https://doi.org/10.1016/j.apsusc.2007.04.083>
  18. D. Tromans, R. Sun, Anodic Polarization Behavior of Copper in Aqueous Chloride/Benzotriazole Solutions, *Journal of The Electrochemical Society*, **138**, 3235 (1991). Doi: <https://doi.org/10.1149/1.2085397>
  19. R. Walker, Benzotriazole as a Corrosion Inhibitor for Immersed Copper, *CORROSION*, **29**, 290 (1973). Doi: <https://doi.org/10.5006/0010-9312-29.7.290>
  20. S.H. Suh, S. Kim, and Y. Suh, Use of Hydrazine for Pitting Corrosion Inhibition of Copper Sprinkler Tubes: Reaction of Hydrazine with Corrosion By-Products, *Corrosion Science and Technology*, **16**, 247 (2017). Doi: <https://doi.org/10.14773/cst.2017.16.5.247>.
  21. S.H. Suh, Y. Suh, H. Kwon, Inhibition of Pitting Corrosion of Copper Tubes in Wet Sprinkler Systems by Sodium Sulfite, *Corrosion Science and Technology*. **16**, 265 (2017). Doi: <https://doi.org/10.14773/cst.2017.16.5.265>.
  22. S. H. Suh, Y. Suh, J. Lee, HS. Kwon, Inhibition of Pitting Corrosion Failure of Copper Tubes in Wet Sprinkler Systems, *Corrosion Science and Technology*, **19**, 82 (2020). Doi: <https://doi.org/10.14773/cst.2020.19.2.89>
  23. D. Tromans, Aqueous Potential-pH Equilibria in Copper/Benzotriazole Systems, *Journal of The Electrochemical Society*, **145**, L42–L45 (1998). Doi: <https://doi.org/10.1149/1.1838335>
  24. U. Bertocci, D. D. Wagman, Standard Potentials in Aqueous Solution, Routledge, NY (2017). Doi: <https://doi.org/10.1201/9780203738764>
  24. D. R. Lide, ed., *Handbook of Chemistry and Physics*, 84th ed., CRC Press (2003).
  26. J.-L. Yao, Y.-X. Yuan, R.-A. Gu, Negative role of triphenylphosphine in the inhibition of benzotriazole at the Cu surface studied by surface-enhanced Raman spectroscopy, *Journal of Electroanalytical Chemistry*, **573**, 255 (2004). Doi: <https://doi.org/10.1016/j.jelechem.2004.07.010>
  27. B. V. Appa Rao, K. Chaitanya Kumar, N. Y. Hebalkar, X-ray photoelectron spectroscopy depth-profiling analysis of surface films formed on Cu–Ni (90/10) alloy in seawater in the absence and presence of 1,2,3-benzotri-

- azole, *Thin Solid Films*, **556**, 337 (2014). Doi: <https://doi.org/10.1016/j.tsf.2014.02.054>
28. T. Kosec, D. K. Merl, I. Milošev, Impedance and XPS study of benzotriazole films formed on copper, copper–zinc alloys and zinc in chloride solution, *Corrosion Science*, **50**, 1987 (2008). Doi: <https://doi.org/10.1016/j.corsci.2008.04.016>